LETTER • OPEN ACCESS

Nanoparticles target early-stage breast cancer metastasis *in vivo*

To cite this article: Evgeniya Goldman *et al* 2017 *Nanotechnology* **28** 43LT01

View the article online for updates and enhancements.

Related content

- Physics of Cancer: The role of macrophages during cancer cell transendothelial migration
  C T Mierke

- Small unilamellar vesicles: a platform technology for molecular imaging of braintumors
  Umar Iqbal, Homam Albaghdadi, Mu-Ping Nieh et al.

- MRI mediated, non-invasive tracking of intratumoral distribution of nanocarriers in ratglioma
  Efstathios Karathanasis, Jaekeun Park, Abhiruchi Agarwal et al.

Letter

Nanoparticles target early-stage breast cancer metastasis *in vivo*

Evgeniya Goldman[1,2]**, Assaf Zinger**[1] **, Dana da Silva**[1]**, Zvi Yaari**[1]**, Ashima Kajal**[1]**, Dikla Vardi-Oknin**[1]**, Mor Goldfeder**[1]**, Josh E. Schroeder**[3]**, Janna Shainsky-Roitman**[1]**, Dov Hershkovitz**[4] **and Avi Schroeder**[1]

[1] Laboratory for Targeted Drug Delivery and Personalized Medicine Technologies, Department of Chemical Engineering, Technion—Israel Institute of Technology, Haifa 32000, Israel
[2] The Interdisciplinary Program for Biotechnology, Technion—Israel Institute of Technology, Haifa, Israel
[3] Department of Orthopedics, Hadassah Medical Center, Jerusalem, Israel
[4] Department of Pathology, Tel-Aviv Sourasky Medical Center, Tel Aviv, Israel

E-mail: avids@technion.ac.il

CrossMark

Abstract

Despite advances in cancer therapy, treating cancer after it has metastasized remains an unmet clinical challenge. In this study we demonstrate that 100 nm liposomes target triple-negative murine breast-cancer metastases post intravenous administration. Metastatic breast cancer was induced in BALB/c mice either experimentally, by a tail vein injection of 4T1 cells, or spontaneously, after implanting a primary tumor xenograft. To track their biodistribution *in vivo* the liposomes were labeled with multi-modal diagnostic agents, including indocyanine green and rhodamine for whole-animal fluorescent imaging, gadolinium for magnetic resonance imaging (MRI), and europium for a quantitative biodistribution analysis. The accumulation of liposomes in the metastases peaked at 24 h post the intravenous administration, similar to the time they peaked in the primary tumor. The efficiency of liposomal targeting to the metastatic tissue exceeded that of a non-liposomal agent by 4.5-fold. Liposomes were detected at very early stages in the metastatic progression, including metastatic lesions smaller than 2 mm in diameter. Surprisingly, while nanoparticles target breast cancer metastasis, they may also be found in elevated levels in the pre-metastatic niche, several days before metastases are visualized by MRI or histologically in the tissue. This study highlights the promise of diagnostic and therapeutic nanoparticles for treating metastatic cancer, possibly even for preventing the onset of the metastatic dissemination by targeting the pre-metastatic niche.

Keywords: nanoparticles, nanotechnology, breast cancer, metastasis, liposome, targeted drug delivery

(Some figures may appear in colour only in the online journal)

Introduction

Breast cancer is the most prevalent cancer among women [1]. The stage at which the disease is diagnosed is an important predictor of prognosis. Up to 99% of patients diagnosed and treated for a confined primary breast cancer tumor will live beyond five years [2]. The prognosis of those diagnosed with

a metastatic disease worsens dramatically, with only 23% of patients surviving beyond five years [2, 3].

Metastasis is defined as one, or multiple, cancer lesions that spread to a tissue that is distant to the primary tumor.

The primary tumor sheds nearly one-million cancer cells per gram tumor every day into circulation [4–6]. A well-established theory is that these circulating cells colonize at distant sites, seeding metastases [6, 7]. The main sites of breast-cancer metastases are the lungs, liver and bone [8]. As the metastases progress, they impair the function of these vital organs.

Common therapeutic options become limited when dealing with metastases [9]. Surgery is extremely effective in treating localized primary tumors but is rarely an option for resecting multiple metastatic lesions [10]. Medication, administered orally or intravenously, may not reach the metastatic sites in sufficient doses to be effective [11, 12]. Targeted therapies and immunotherapies offer a new and promising avenue for treating the metastatic disease [13–15]. Specifically, nanotechnologies that are targeted simultaneously to multiple metastatic sites in the body while carrying small-molecule drugs, proteins, nucleic acids or imaging agents, will enable management of metastatic cancer [16–26].

In this study, we assessed the ability of nanoparticles to target triple-negative breast cancer (TNBC) metastases *in vivo*. TNBC is characterized by the lack of expression of two hormone receptors (estrogen and progesterone) and a deficiency of human epidermal growth factor receptor 2 (HER2). These cell-surface receptors are utilized for targeting medicines to the cancerous lesions. In their absence, TNBC has limited treatment options and a poor prognosis [27].

Targeting nanoparticles to cancerous tissues can exploit physical or biological mechanisms [28–34], one of which is targeting the leaky vasculature in cancerous tissue [35, 36]. In contrast to normal tissues, solid tumors undergo unregulated angiogenesis, providing the tumor with vasculature to supply the metabolic needs of the rapidly dividing cancerous cells [37]. The resultant blood vessels exhibit a discontinuous endothelial-cell lining, with gaps ranging from 200 to 2000 nm between individual endothelial cells [38–40]. The poor architecture of the tumor vasculature is an access point for therapeutic nanoparticles circulating in the blood [41]. In order to penetrate the tumor, the nano dimensions of the drug carriers must be smaller than the size of the pores in the vasculature. Experimental studies show that particles smaller than 150 nm are advantageous for tumor penetration [8, 42]. Once the nanoparticles penetrate the tumor vasculature, they are taken up by cells [43], or are retained in the extracellular matrix. Nanoparticles are usually not trafficked out of the tumor region, because of the impaired lymphatic drainage in tumors [44–46]. This phenomenon, in which nanoparticles accumulate in cancerous tissues post intravenous administration, has been coined the enhanced permeability and retention (EPR) effect, or passive targeting [47–49].

In breast cancer, the EPR effect is leveraged clinically to target nanomedicines to the primary tumor [48, 50–52].

In total, nearly 250 nanotechnologies have either been approved or are in advanced approval stages by the FDA and EMA for treating a wide range of diseases, including breast cancer [53–59]. For example, Doxil is a 100 nm PEGylated liposome formulation loaded with the chemotherapeutic agent doxorubicin, and is used in first-line breast cancer management [60]. PEG (polyethylene glycol) on the surface of the liposomes increases their half-life in the circulation and reduces the uptake of the nanoparticle by the mononuclear phagocyte system [48, 61]. These liposomes were shown to target tumors in patients [48], while reducing life-threatening side-effects, such as cardiomyopathy [62]. Another clinical nanotechnology used for breast cancer treatment is Abraxane —130 nm albumin nanoparticles loaded with the microtubule inhibitor paclitaxel [63].

In this study, we examined whether intravenously injected PEGylated liposomes can target breast cancer metastases. We studied the effect of several disease conditions on nanoparticle accumulation at the metastatic site, including the size of the metastases, the presence or absence of a primary tumor alongside the metastases, and the size of the metastatic lesion.

Materials and methods

Study design

This study compared the biodistribution of 100 nm liposomes to the primary tumor and metastasis, post intravenous injection. Three disease models were compared to mirror the clinical scenario: (1) tumor alone, mimicking the existence of a primary tumor; (2) metastasis alone, mimicking metastatic development after resection of the primary tumor; and (3) tumor plus induced lung metastasis, mimicking an advanced stage of the disease (figure 1).

Liposome preparation

Liposomes were prepared as previously described [64]. Briefly, liposomes were composed of 55 mole% hydrogenated soybean phosphatidylcholine (HSPC; Lipoid, Ludwigshafen, Germany); 40 mole% cholesterol (Sigma-Aldrich) and 5 mole% PEG distearoyl-phosphoethanolamine (m2000PEG-DSPE, MW 2810; Lipoid). For sulforhodamine-labeled liposomes, 0.04 mole% of 1,2-dipalmitoyl-sn-glycero-3-phosphoethanolamine-N-lissamine rhodamine B sulfonyl-ammonium salt (16:0 Liss Rhod PE; Avanti Polar Lipids, Alabaster, Alabama) were added.

The lipids were dissolved in chloroform. The solvent was then evaporated under reduced pressure at 55 °C, 100 mbar, using a R-210 Rotorvaporator (Buchi, Switzerland). The dry lipid film was then hydrated with 5% w/v dextrose or phosphate buffered saline (PBS), depending on the entrapped molecule (see below), to reach a final lipid concentration of 50 mM.

Contrast agent molecules used in this study included indocyanine green dye (ICG, Sigma-Aldrich) [65], 0.13 mM in 5% w/v dextrose; europium chloride hexahydrate (Eu,
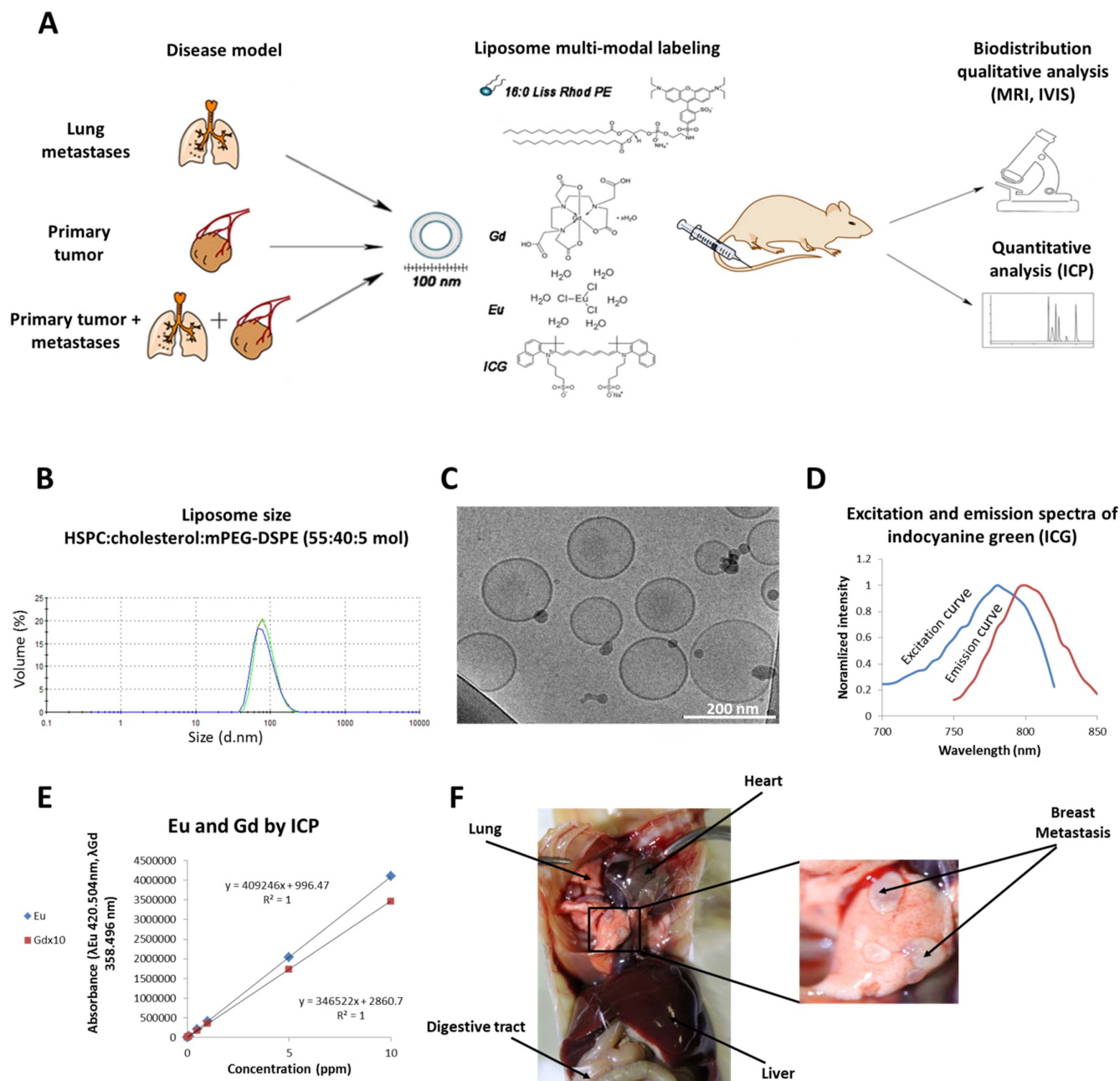
Figure 1. Metastatic models and liposome characterization. (A) 100 nm liposomes were loaded with rare earths and contrast agents, and their biodistribution to triple-negative breast cancer (TNBC) metastasis, primary TNBC tumors, or both, were evaluated quantitatively and qualitatively in mice. Liposomes were loaded with traces of rare-earths and clinical contrast agents, including indocyanine green (ICG), rhodamine, gadolinium (Gd) and europium (Eu). The liposomal biodistribution to the cancerous tissues was evaluated quantitatively, using ICP, and qualitatively, by MRI and whole-animal fluorescent imaging. Liposomes were sized around 100 nm using dynamic light scattering (B) and cryoTEM microscopy (C). ICG-liposomes have a far-red fluorescent emission that can be detected in the cancerous tissue (D). Metastatic levels of Eu and Gd were measured analytically by ICP (E) or using MRI. Experimental TNBC lung metastases occur in BALB/c mice after injecting 4T1 cells intravenously (F). The metastatic lesions have a white, blister-like, appearance within the pink lung tissue.

Sigma-Aldrich, [66]), 185 mM in 5% w/v dextrose; and gadopentetic acid (Gd, Sigma-Aldrich), 500 mM in PBS.

To produce nanoscale vesicles, the liposomes were extruded (Lipex Extruder, Northern Lipids, Vancouver, Canada) in a stepwise manner at 60 °C through polycarbonate membrane filters (Whatman, Newton, USA) with 400, 200, and 100 nm pores. Four extrusion steps were applied per filter type. After extrusion, the liposome suspension was dialyzed against 5% w/v dextrose or PBS solution using a 12–14 kDa dialysis tube to remove non-entrapped materials.

Liposome size distribution was measured by dynamic light scattering using a Zetasizer Nano ZSP (Malvern Instruments, UK). Samples were diluted 1–100 in the appropriate buffer. Sizing measurements were conducted at room temperature and the back-scattered light was detected at an angle of 173°.

CryoTEM imaging of the liposomes was performed as follows: lipid dispersions at concentration of 5 mM are prepared in a controlled-environment vitrification system at 25 °C and 100% relative humidity and examined in a Philips CM120 cryo-electron microscope operated at 120 kV. Specimens were equilibrated in the microscope below –178 °C, then examined in the low-dose imaging mode to minimize electron beam radiation damage, and recorded at a nominal under-focus of 4–7 nm to enhance phase contrast an Oxford CT-3500 cooling holder was used. Images were recorded digitally by a Gatan MultiScan 791 CCD camera using the Digital Micrograph 3.1 software package (Gatan).

ICG entrapment was determined using an Infinite 200PRO multimode plate reader (Tecan, Switzerland), excitation/emission 780/810 nm. For this, the liposomes were dissociated using the Bligh and Dyer method [67]. Briefly, liposomes were diluted in the volume ratio of liposome:chloroform:methanol:water of 0.8:2:2:1 in order to obtain two separate phases; (1) an organic phase that contained all the lipids and (2) an aqueous phase that contained all the water-soluble materials. The absorbance of the ICG in water phase was measured.

Eu/Gd entrapment was determined using inductively coupled plasma optical emission spectroscopy (ICP-OES, 5100 system, Agilent Technologies, US). The amount of metal was calculated using a calibration curve according to Europium/Gadolinium ICP standards (Sigma-Aldrich, Rehovot, Israel).

Cell culture

A TNBC cell line, 4T1 (ATCC), was used to induce primary tumors and metastasis. Cells were cultured at 37 °C in a humidified atmosphere and 5% CO_2 in air. RPMI 1640 medium, supplemented with 10% heat inactivated Fetal Bovine Serum, 1% v/v Penicillin-Streptomycin solution (10 000 U ml^{-1} of Penicillin G Sodium Salt and 10 mg ml^{-1} of Streptomycin Sulfate), and 1% v/v L-Glutamine (all from Biological Industries, Beit Haemek, Israel). The cells were washed thoroughly with PBS at 4 °C before injection.

In vivo

All animal studies were approved and performed according to the guidelines of the Institutional Animal Research Ethical Committee at the Technion—Israel Institute of Technology. Animal welfare was monitored daily both by the researchers and staff veterinarians.

Eight to ten-week-old ($\sim$20 gr) BALB/c female mice (Harlan laboratories, Jerusalem, Israel) were used for all animal models.

Inducing primary tumors. 1×10^6 4T1 cells in 100 μl of PBS were injected subcutaneously (SC) into the rear right flank; 500 mm^3 tumors developed approx. 14 d post injection.

Experimental metastasis. 2×10^5 4T1 cells in 100 μl of PBS were injected intravenously (IV) via the tail vein; lung metastasis developed 14 d post injection.

Combined primary tumor and metastasis. 2×10^5 4T1 cells in 100 μl of PBS were injected IV, to form metastases; and an additional 7×10^5 4T1 cells in 100 μl of PBS were injected SC, to form the primary tumor. Both the primary tumor and metastasis formed $\sim$14 d post injection.

Spontaneous metastasis and the pre-metastatic niche. 5×10^5 4T1 cells in 100 μl of PBS were injected SC to the rear right flank to induce the formation of a primary tumor, metastasis evolved spontaneously in the lungs 3–4 weeks later. During the time between the induction of the primary tumor and the histological detection of metastases, a pre-metastatic niche is formed in the lung, conditioning this tissue to harbor the disseminated metastatic cells.

Quantitative biodistribution analysis

Once the metastases evolved mice were injected intravenously with 300 μl Gd-loaded liposomes (100 nm, 50 mM lipid). Twenty-four hours after the injection, the mice were sacrificed and the metastatic lesions were excised and analyzed for the liposome presence using Gd ICP analysis.

MR imaging

MRI scans were acquired using a 1 T micro-MRI (Aspect M2 MRI, Aspect Imaging, Modi'in, Israel) equipped with a cylindrical radiofrequency volume coil (35 mm inner diameter) for signal excitation and reception. During imaging the animal was placed in a coronal position on a holder and kept anaesthetized with 0.5%–1.5% Isoflurane, supplemented with oxygen (0.8 l min^{-1}) via a facial mask. The respiratory rate of the mice was monitored using a pressure pad (Aspect M2, Aspect Imaging, Israel) located on the abdomen.

Two scan sets, T2 and T1 weighted, were acquired for each animal: (i) FSE (Fast Spin Echo) sequence, slice thickness = 0.9 mm, slice gap = 0.1 mm, FOV = 5 × 5 cm, matrix dimension = 200 × 200, spatial resolution = 250 × 250 μm^2, repetition/echo time (TR/TE) = 2253/53 ms, number of excitations = 2, number of averages = 4; and (ii) GRE-SP (Gradient Echo) sequence, slice thickness = 1 mm, FOV = 5 × 5 cm, matrix dimension = 200 × 200, spatial resolution = 250 × 250 μm^2, repetition/echo time (TR/TE) = 12.6/3.2 ms, number of excitations = 6.

Image processing was performed using MRI image analysis and a MATLAB based software (MRItool). For each image, regions of interest in the lungs were manually segmented to measure the total signal intensity, average signal, and area.

Fluorescent imaging

100 μl ICG liposomes (100 nm, 50 mM lipid) or the same amount of free (non-liposomal) ICG was injected IV via the mouse tail vein. Animals were sacrificed at time intervals of 0, 3, 6, 12, 24, and 48 h post injection, and the metastatic lungs and or tumors were excised and imaged using a MaestroEX *in vivo* fluorescent imaging system equipped with an excitation filter at 690 nm. A 750 nm long-pass emission filter was applied to prevent the interference of excitation light with the charge coupled device (CCD) camera. *In vivo* spectral imaging from 780 to 820 nm (in 10 nm steps) was carried out with an exposure time of 5000 ms for each image frame. Background was removed by using the spectral unmixing software (Maestro 2p20).

Gd-rhodamine liposomes (enabling dual imaging modalities; Gd—MRI; and rhodamine—fluorescent) were injected IV (300 μl); 24 and 48 h after the injection mice were scanned by MRI, then the lungs were resected and analyzed histologically to visualize the exact tissue deposition of the liposomes [68].

Quantification of Eu and Gd delivery to tumor and metastasis

After imaging, organ samples were washed thoroughly with PBS, dried and weighed. Europium (Eu) or Gadolinium (Gd) content in the organs was quantified using ICP. For this purpose samples were carbonized at 500 °C for 5 h and their ash was dissolved in nitric acid 1% v/v (Bio Labs, Israel).

Histology

After sacrificing the mice, the lungs were removed and kept in 10% neutral buffered formalin (Sigma) at room temperature. Later, the tissues were paraffin embedded and sectioned into 5 μm slides. Slides were stained with hematoxylin and eosin (H&E) to evaluate the general morphology and further stained with 4′,6-diamidino-2-phenylindole (DAPI) for fluorescence imaging.

All data groups we analyzed statistically using an unpaired, two-sided Student's t-test. Confidence level was taken to be $P = 0.05$.

Results and discussion

Breast cancer is a global epidemic [69], of which the metastatic condition is the most lethal [70]. Nearly 250 000 patients are diagnosed annually with metastatic breast cancer in the US alone, and more than 40 000 die of this condition [71]. In developing countries too, numbers of breast cancer patients are increasing as life span, awareness to cancer and medical infrastructures are improving [72, 73]. Diagnosing and treating metastatic TNBC, a subtype of breast cancer, is especially challenging, due to the lack of biological drugs that can target this condition [74].

In this study, we investigated whether 100 nm liposomes can target TNBC metastases *in vivo*.

Three murine disease models that mirror relevant clinical scenarios were studied: (1) Targeting a primary tumor alone —modeling the early stages of the disease; (2) Targeting metastasis alone—modeling the metastatic disease after a primary tumor has been resected; and, (3) Targeting both the metastases and a primary tumor simultaneously—modeling a metastatic disease with a non-resected primary tumor (figure 1(A)). In addition, two complementary experimental approaches were employed to induce metastases. The first is 'experimental metastasis', in which triple-negative (4T1) cancer cells are injected intravenously to induce lung metastases in BALB/c mice [75–77]. Experimental metastasis is commonly used because of its experimental reproducibility [75, 78]. Moreover, we studied nanoparticle biodistribution to a 'spontaneous metastatic model', in which a primary 4T1 tumor xenograft was implanted in mice, spontaneously seeding distant metastases [75].

We first studied the ability of 100 nm liposomes to accumulate in primary breast cancer tumors. For this, we compared the biodistribution of liposomes loaded with ICG (a clinical contrast agent) to an equal amount of free ICG injected intravenously (figure 2(A)). Animals injected with the free dye had a maximal fluorescent signal in the primary tumor 3 h post intravenous administration, after which the signal decayed (figure 2(B)). In comparison, the accumulation of liposomes peaked in the tumor after 24 h. The intensity of the fluorescent signal in tumors of mice injected with the ICG-liposomes was 4.5-fold greater than the maximal signal in tumors of mice injected with the free dye [79]. These data confirm previous findings that nanoparticulate systems have an advantage over the free small molecules in accumulating in primary tumor [35, 48, 80]. The mechanism governing nanoparticle biodistribution to primary tumors has been shown to be dependent on the nanoparticles' half-life in circulation as well as their ability to extravasate through the compromised tumor vasculature [81–85]. PEG conjugated to the corona of the liposomes extends the liposomes' circulation time *in vivo* [86], and their nano-dimensions facilitates extravasation through the compromised tumor vasculature [87, 88].

After confirming the liposomes were detected in the primary tumor, we tested whether 100 nm liposomes can also be detected in the metastasis post intravenous administration. For this, experimental TNBC metastasis was induced in the lungs of BALB/c mice. Liposomes containing ICG or free ICG were injected intravenously, and the mice were imaged over 48 h. A fluorescent signal was detected in the metastatic lungs after the injection (figure 2(A)). Similar to the primary tumor, the free dye biodistribution in the metastases peaked after 3 h and the nanoparticles peaked at 24 h post intravenous injection (figure 2(C)). The similar kinetics in the primary tumor and metastases, suggest that a similar mechanism governs accumulation in both, namely, extravasation of the nanoparticles from the circulation into the metastatic lesions [89, 90]. If the patient is diagnosed after cancer has already metastasized, the primary tumor is usually not resected [91–96]. To this end, we studied the liposome accumulation in metastasis in the presence, or absence, of a primary tumor.
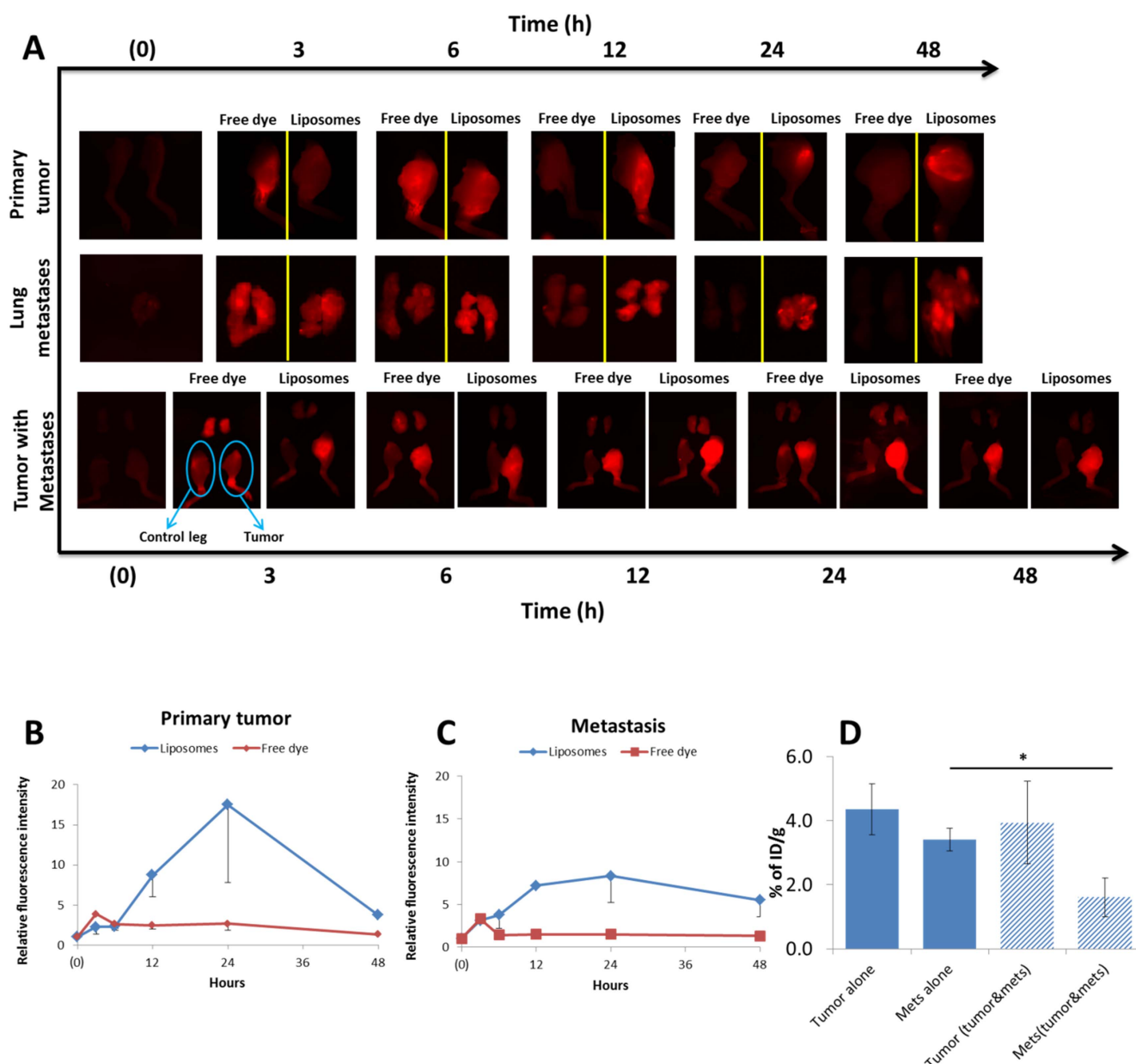
Figure 2. Nanoparticles accumulate in primary tumors and lung metastasis 24 h after intravenous injection. (A) Indocyanine green (ICG)-containing liposomes, or free ICG, was injected intravenously to BALB/c mice and the biodistribution to the primary tumors and metastases was tracked using whole-animal fluorescent imaging. The intensities of the fluorescent ICG signals were measured in the primary tumor (B) and metastases (C). The accumulation of Eu-loaded liposomes in metastases, in the presence or absence of a primary tumor, was compared 24 h post injection (D). (0) indicates imaging before the liposomes were injected. Data is shown as the mean $\pm$ SDE of $n = 5$; $^{*}P < 0.05$. Differences between two means were tested using an unpaired, two-sided student's t-test.

The presence of a primary tumor decreased liposome accumulation at the metastatic site (figure 2(D)). The accumulation of the liposomes in metastases, in the absence of a primary tumor reached 3.4% $\pm$ 0.3% of the injected dose per gram tissue. In comparison, when the primary tumor coexisted with the metastasis, the accumulation of the liposomes in the metastasis declined to 1.6% $\pm$ 0.6% (figure 2(D)). This is explained by a sink effect the primary tumor has on liposomal biodistribution, in which liposomes are deterred from the circulation to the primary tumor reducing their accumulation in the metastasis [5, 38, 97–101]. Furthermore, previous studies have demonstrated that the primary tumor suppresses vascular progression in the disseminated metastasis [102–106], thereby possibly reducing the ability of liposomes to extravasate from the capillaries into the metastasis [107]. While in the clinical scenario, there is controversy whether resection of the primary tumor in patients with metastatic breast cancer improves prognosis [91–95]. Our data suggest that nanoparticles target metastases more effectively in the absence of a primary tumor.

While fluorescent imaging is used mainly for pre-clinical cancer research, MRI is a common imaging modality for diagnosing cancer clinically. We tested whether nanoparticles can also be detected in the metastatic lesions by MRI and their
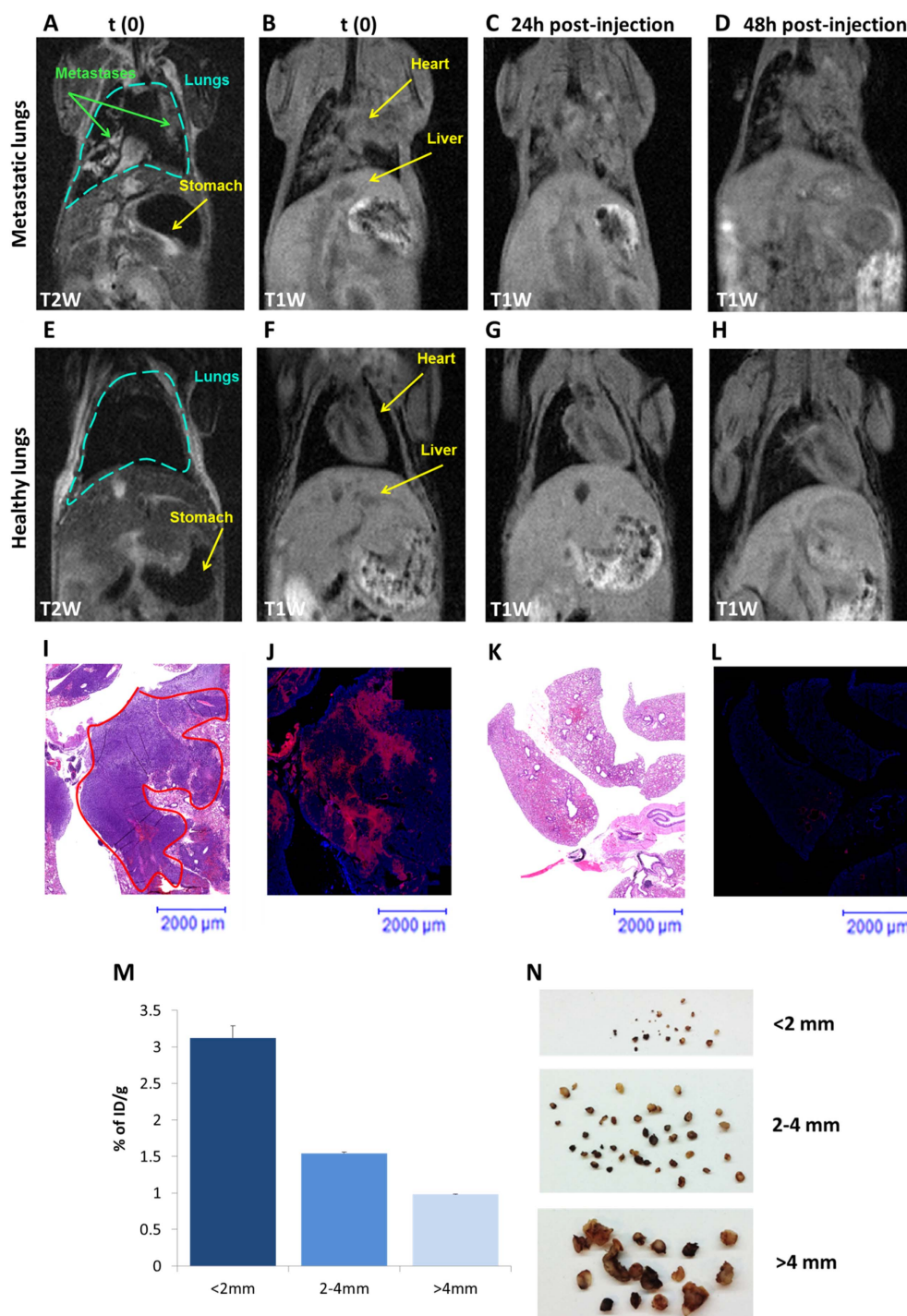
Figure 3. Nanoparticles accumulate in millimeter-sized lung metastases. The localization of liposomes inside the metastatic tissue was examined. Gd-liposomes were injected intravenously to metastases-bearing or to healthy mice. Mice were scanned by MRI prior to, 24 and 48 h after the particle injection. The lungs were then excised and analyzed histologically. MRI scans of metastases-bearing (A)–(D) or healthy (E)–(H) BALB/c mice were taken prior to, 24 h, and 48 h after intravenous administration of Gd-liposome. The lung anatomy is marked with the discontinuous green line while the gray accumulation of the Gd-liposomes in the lungs can be noticed in the diseased mice. (C) and (D) 24 h and 48 h (respectively) post Gd liposomes injection. MRI images show an enhanced signal from the metastatic lungs (gray areas are due to enhanced liposome accumulation in the metastatic sites). Histology. Rhodamine-labeled liposomes were injected intravenously to metastases-bearing and healthy mice. Twenty-four hours later the lungs were excised. H&E and fluorescent images of the metastatic (I), (J) and healthy (K), (L) lungs, respectively. The accumulation of the fluorescent red liposomes can be noticed in the metastatic tissue (J), while the healthy tissue displayed only the blue DAPI nuclei staining. (M), (N) Liposome accumulation in metastatic lesions as a function of the size of metastases. Mice bearing lung metastases were administered 100 nm Gd-liposomes intravenously. Twenty four hours later, the lungs were excised, and the individual metastatic lesions were resected, and divided into three groups according to their sizes (M). The Gd content in each group was quantified using ICP (N). Data is shown as the mean ± SD.
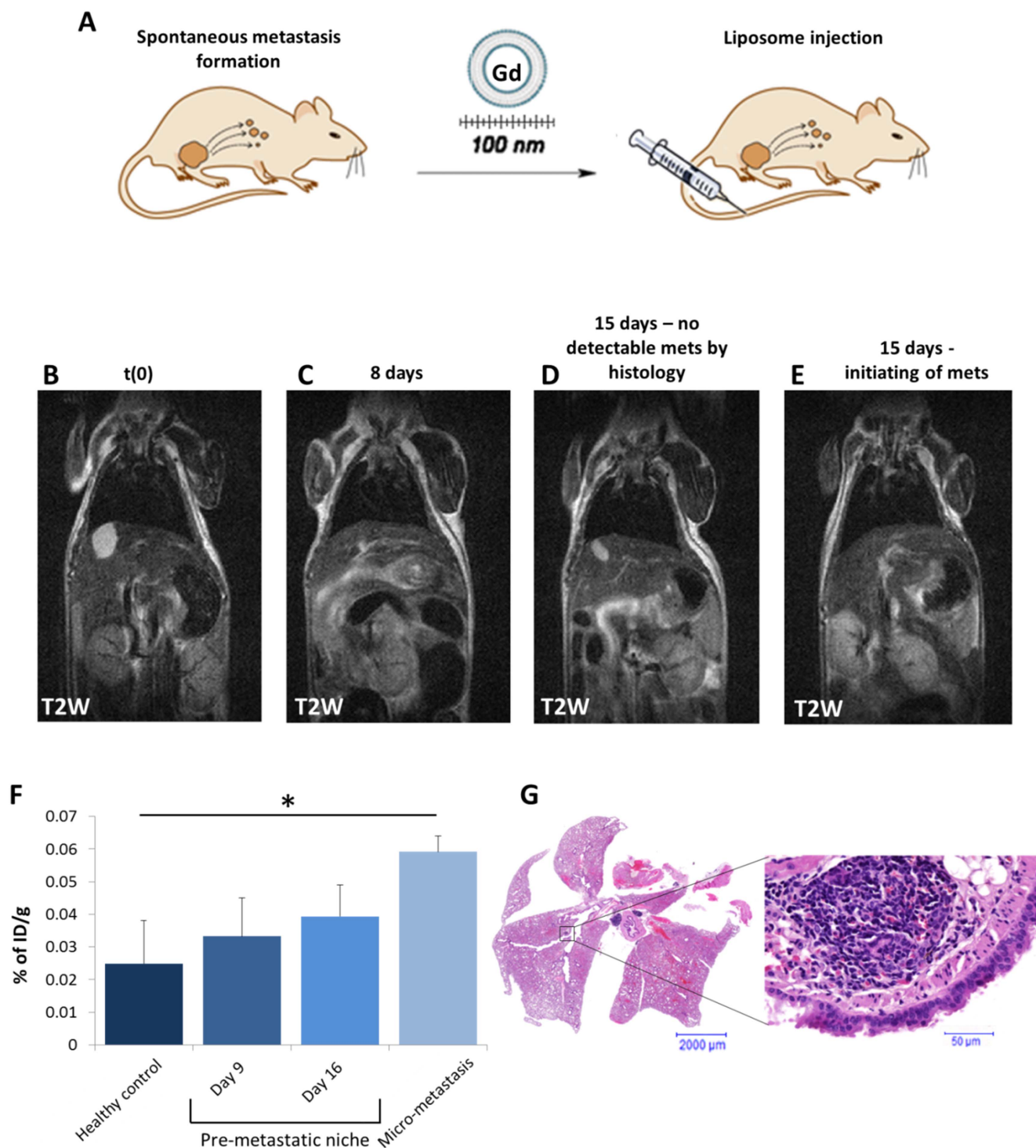
Figure 4. Liposomes accumulate in the pre-metastatic niche. (A) Spontaneous metastasis can be detected in the lungs of mice approximately three weeks after implanting a primary tumor. Before the metastases can be detected histologically or by imaging, the pre-metastatic lungs are conditioned to harbor the metastatic cells. We examined the ability of liposomes to target the pre-metastatic niche in the lungs, i.e. the lung tissues before metastasis could be detected in them by imaging. Mice were scanned throughout the study using MRI: before inducing the primary tumor (B), on day 8 (C), and day 15 (D). None of the mice presented detectable metastases by MRI (B)–(D). Gd-loaded liposomes were administered intravenously after the MRI scans. Twenty-four hours post injection the mice were sacrificed, lungs were excised and evaluated histologically for the presence of micro-metastases that were not detected by MRI, and by ICP for a quantitative analysis of the presence of Gd-liposomes. ICP analysis indicated that the accumulation of Gd-liposomes increased in the lungs as the time since induction of the primary tumor increased (F). In some mice, micro-metastases were visualized histologically (G), even though they were undetectable by MRI (E). Lungs diagnosed histologically with micro-metastases (G) had greater amounts of Gd-liposomes compared to pre-metastatic lungs (F). Data are shown as the mean $\pm$ SDE of $n = 2$ (control), $n = 6$ (day 8), $n = 4$ (day 15), $n = 2$ (mets initiating); $^*p = 0.074$. Differences between two means were tested using an unpaired two-sided Student's t-test.

presence in the metastasis subsequently confirmed histologically by fluorescent-histology of the tissue. For this, we replaced the fluorescent ICG inside the liposomes with an MRI contrast agent—gadolinium (Gd) [68]. In addition, we doped the liposome membrane with sulforhodamine-lipids, generating a multi-modal (fluorescence and MRI) diagnostic liposome. A bright co-localization signal of the Gd-liposomes inside the metastatic lesions was recorded by MRI 24 h after the intravenous injection (figures 3(A)–(D)). The same experiment carried out in healthy mice showed no Gd-liposomes signal in the lungs (figures 3(E)–(H)). The accumulation of Gd-liposomes in the metastatic lesions was confirmed histologically. For this, the metastatic lungs were resected and stained with H&E. The liposomal rhodamine signal coincided with metastatic lesions (figure 3(J)). A fluorescent signal was not found in the lungs of healthy animals (figure 3(L)). These data confirmed our initial whole-animal fluorescent imaging findings that 100 nm liposomes injected intravenously accumulate in the metastatic tissue (figure 1), and indicated that liposomes can be used as MRI contrast agents for imaging metastasis.

One major requirement from nanoparticles is the ability to target small metastatic lesions [101, 108]. For this, we quantified the accumulation of nanoparticles in metastases of different sizes: smaller than 2 mm, between 2 and 4 mm, and larger than 4 mm. Metastases were induced experimentally in the lungs of BALB/c mice by an intravenous injection of 4T1 cells. Once the metastases were detected by MR imaging, mice were injected 100 nm Gd-loaded liposomes intravenously. Twenty-four hours later, the mice were sacrificed, lungs were excised, and the individual metastatic lesions were resected and grouped according to size (figures 3(M), (N)). All three metastasis groups (<2 mm, 2–4 mm, and >4 mm) had significant Gd-liposomal presence. Higher levels of nanoparticle accumulation were detected in the smallest metastasis, reaching $3.1\% \pm 0.2\%$ of the injected dose per gram tumor in lesions smaller than 2 mm in diameter, compared to $1.5\% \pm 0.02\%$ and $1.0\% \pm 0.01\%$ in the 2–4 mm and >4 mm groups, respectively (figure 3(M)). The higher accumulation of nanoparticles in the smaller lesions is explained by higher vascular density and permeability in the smaller lesions [109–111]. Similar tendencies, in which nanoparticle' accumulation per gram tumor increases as the lesion size decreases, was reported also in primary tumors [112]. It should also be noted that 2 mm lesions are below the limit-of-detection of most clinical imaging systems, thereby targeting imaging agents to such small lesions can facilitate early metastatic detection [113].

Before metastases colonize in a healthy organ, biochemical signals are sent from the primary tumor, to enable the metastatic cells to adhere and progress at the distant metastatic site [7, 114]. During this process the vasculature at the destination organ becomes leaky [115]. Since lungs are a primary site of metastatic dissemination, we tested whether nanoparticles can be detected in the pre-metastatic lungs [8]. For this, a primary tumor was implanted in the rear flank of BALB/c mice (figure 4(A)). One and two weeks post-implantation of the primary tumor the mice were scanned

using MRI. No metastatic malignancy was detected by MRI in the lungs (figures 4(B)–(E)). At these time points, mice were injected with 100 nm Gd-liposomes intravenously. Twenty four hours later (day 9 or day 16), mice were sacrificed and the lungs were excised and fixated. All the histological slides were evaluated as normal (no evidence of metastasis), except for two slides that showed foci of isolated tumor cells (micro-metastasis, <0.2 mm, figure 4(G)). After the histological analysis, the tissue blocks were digested and analyzed for the presence of Gd-liposomes using ICP. A gradual elevation in the levels of Gd was detected in the pre-metastatic lungs compared to the healthy lungs over time (figure 4(F)). Lungs that were evaluated histologically with micro-metastasis had greater concentrations of Gd-liposomes, reaching 0.059% of the injected dose. Having this said, using an unpaired two-sided student t-test, we did not reach the statistical level of significance we hoped for nanoparticle detection in the pre-metastatic niche ($p = 0.074$ versus $p < 0.05$). This is explained by the inefficiency of the metastatic process, and the limit-of-detection of the existing analytical tools. In metastasis, only 0.01% of the circulating tumor cells colonizes at the metastatic site and form viable metastases [4–6, 9, 116–118]. Respective to the injected nanoparticles, 0.01% of the injected dose is 1.2 nM Gd, which is near the limit of detection of Gd by ICP (0.3 ppb). This explains the lower level of confidence of detection in the pre-metastatic niche, rendering the development of more accurate systems for studying nanoparticle distribution to the pre-metastatic niche.

These results suggest that nanoparticles accumulate preferentially in the pre-metastatic lungs. This is explained by biological conditioning of the lung tissue for the emergence of metastases [7, 9, 114, 115, 119–121]. During this process the vasculature at the target organ becomes hyper-permeable [115], enabling nanoparticle accumulation in the pre-metastatic lungs [120, 122, 123].

Ultimately, when a patient is diagnosed with a primary tumor, the main concern is preventing future metastatic dissemination. Our data suggest that even before having imaging evidence of the existence of metastatic lesions in an organ, the pre-metastatic niche may be targeted and treated with nanoparticles; thereby, possibly, preventing future metastatic progression at this site.

In summary, this study demonstrates that 100 nm liposomes target triple negative murine breast cancer metastasis. Our findings support the use of nanotechnology for imaging and targeting medicines to metastases and ultimately to the pre-metastatic niche.

Acknowledgments

ORCID iDs

Assaf Zinger https://orcid.org/0000-0001-7894-486X

References

[1] Siegel R L, Miller K D and Jemal A 2016 Cancer statistics, 2016 *CA: Cancer J. Clinicians* **66** 7–30

[2] Horner M *et al* 2009 *SEER Cancer Statistics Review, 1975–2006* (Bethesda, MD: National Cancer Institute)

[3] DeSantis C, Siegel R, Bandi P and Jemal A 2011 Breast cancer statistics, 2011 *CA: Cancer J. Clinicians* **61** 409–18

[4] Butler T P and Gullino P M 1975 Quantitation of cell shedding into efferent blood of mammary adenocarcinoma *Cancer Res.* **35** 512–6

[5] Chang Y S, di Tomaso E, McDonald D M, Jones R, Jain R K and Munn L L 2000 Mosaic blood vessels in tumors: frequency of cancer cells in contact with flowing blood *Proc. Natl Acad. Sci. USA* **97** 14608–13

[6] Hosseini H *et al* 2016 Early dissemination seeds metastasis in breast cancer *Nature* **540** 552–558

[7] Massague J and Obenauf A C 2016 Metastatic colonization by circulating tumour cells *Nature* **529** 298–306

[8] Schroeder A, Heller D A, Winslow M W, Dahlman J E, Pratt G W, Langer R, Jacks T and Anderson D G 2011 Treating metastatic cancer with nanotechnology *Nat. Rev. Cancer* **12** 39–50

[9] Valastyan S and Weinberg R A 2011 Tumor metastasis: molecular insights and evolving paradigms *Cell* **147** 275–92

[10] Harris E, Barry M and Kell M R 2013 Meta-analysis to determine if surgical resection of the primary tumour in the setting of stage IV breast cancer impacts on survival *Ann. Surg. Oncol.* **20** 2828–34

[11] Minchinton A I and Tannock I F 2006 Drug penetration in solid tumours *Nat. Rev. Cancer* **6** 583–92

[12] Hryniuk W and Bush H 1984 The importance of dose intensity in chemotherapy of metastatic breast cancer *J. Clin. Oncol.* **2** 1281–8

[13] Slamon D J *et al* 2001 Use of chemotherapy plus a monoclonal antibody against HER2 for metastatic breast cancer that overexpresses HER2 *New Engl. J. Med.* **344** 783–92

[14] Demaria S, Kawashima N, Yang A M, Devitt M L, Babb J S, Allison J P and Formenti S C 2005 Immune-mediated inhibition of metastases after treatment with local radiation and CTLA-4 blockade in a mouse model of breast cancer *Clin. Cancer Res.* **11** 728–34

[15] Ofek P, Fischer W, Calderon M, Haag R and Satchi-Fainaro R 2010 *In vivo* delivery of small interfering RNA to tumors and their vasculature by novel dendritic nanocarriers *FASEB J.* **24** 3122–34

[16] Shamay Y *et al* 2016 P-selectin is a nanotherapeutic delivery target in the tumor microenvironment *Sci. Trans. Med.* **8** 345ra387

[17] Lammers T, Kiessling F, Ashford M, Hennink W, Crommelin D and Storm G 2016 Cancer nanomedicine: is targeting our target? *Nat. Rev. Mater.* **1** 16069

[18] Stark W J 2011 Nanoparticles in biological systems *Angew. Chem., Int. Ed. Engl.* **50** 1242–58

[19] Lellouche E *et al* 2015 MagRET nanoparticles: an iron oxide nanocomposite platform for gene silencing from MicroRNAs to long noncoding RNAs *Bioconjug. Chem.* **26** 1692–701

[20] Fleige E, Quadir M A and Haag R 2012 Stimuli-responsive polymeric nanocarriers for the controlled transport of active compounds: concepts and applications *Adv. Drug. Deliv. Rev.* **64** 866–84

[21] Weissleder R, Nahrendorf M and Pittet M J 2014 Imaging macrophages with nanoparticles *Nat. Mater.* **13** 125–38

[22] Ferrari M 2005 Cancer nanotechnology: opportunities and challenges *Nat. Rev. Cancer* **5** 161–71

[23] Anchordoquy T J *et al* 2017 Mechanisms and barriers in cancer nanomedicine: addressing challenges, looking for solutions *ACS Nano* **11** 12–8

[24] Kaneti L, Bronshtein T, Malkah Dayan N, Kovregina I, Letko Khait N, Lupu-Haber Y, Fliman M, Schoen B W, Kaneti G and Machluf M 2016 Nanoghosts as a novel natural nonviral gene delivery platform safely targeting multiple cancers *Nano Lett.* **16** 1574–82

[25] Zimmerman J F, Parameswaran R, Murray G, Wang Y, Burke M and Tian B 2016 Cellular uptake and dynamics of unlabeled freestanding silicon nanowires *Sci. Adv.* **2** e1601039

[26] Shapira A, Kim D H and Dvir T 2014 Advanced micro- and nanofabrication technologies for tissue engineering *Biofabrication* **6** 020301

[27] Dawood S 2010 Triple-negative breast cancer: epidemiology and management options *Drugs* **70** 2247–58

[28] Kedmi R and Peer D 2016 Zooming in on selectins in cancer *Sci. Trans. Med.* **8** 345fs311

[29] Peer D, Karp J M, Hong S, Farokhzad O C, Margalit R and Langer R 2007 Nanocarriers as an emerging platform for cancer therapy *Nat. Nanotechnol.* **2** 751–60

[30] Torchilin V P 2014 Multifunctional, stimuli-sensitive nanoparticulate systems for drug delivery *Nat. Rev. Drug Discovery* **13** 813–827

[31] Jakobsohn K, Motiei M, Sinvani M and Popovtzer R 2012 Towards real-time detection of tumor margins using photothermal imaging of immune-targeted gold nanoparticles *Int. J. Nanomed.* **7** 4707–13

[32] Rizzo L Y, Theek B, Storm G, Kiessling F and Lammers T 2013 Recent progress in nanomedicine: therapeutic, diagnostic and theranostic applications *Curr. Opin. Biotechnol.* **24** 1159–66

[33] Peer D and Margalit R 2004 Tumor-targeted hyaluronan nanoliposomes increase the antitumor activity of liposomal doxorubicin in syngeneic and human xenograft mouse tumor models *Neoplasia* **6** 343–53

[34] de la Fuente M, Ravina M, Sousa-Herves A, Correa J, Riguera R, Fernandez-Megia E, Sanchez A and Alonso M J 2012 Exploring the efficiency of gallic acid-based dendrimers and their block copolymers with PEG as gene carriers *Nanomedicine* **7** 1667–81

[35] Matsumura Y and Maeda H 1986 A new concept for macromolecular therapeutics in cancer chemotherapy: mechanism of tumoritropic accumulation of proteins and the antitumor agent smancs *Cancer Res.* **46** 6387–92

[36] Shi J, Kantoff P W, Wooster R and Farokhzad O C 2017 Cancer nanomedicine: progress, challenges and opportunities *Nat. Rev. Cancer* **17** 20–37

[37] Miller K, Eldar-Boock A, Polyak D, Segal E, Benayoun L, Shaked Y and Satchi-Fainaro R 2011 Antiangiogenic antitumor activity of HPMA copolymer-paclitaxel-alendronate conjugate on breast cancer bone metastasis mouse model *Mol. Pharm.* **8** 1052–62

[38] Naumov G N, Akslen L A and Folkman J 2006 Role of angiogenesis in human tumor dormancy: animal models of the angiogenic switch *Cell Cycle* **5** 1779–87

[39] Carmeliet P and Jain R K 2000 Angiogenesis in cancer and other diseases *Nature* **407** 249–57

[40] Hobbs S K, Monsky W L, Yuan F, Roberts W G, Griffith L, Torchilin V P and Jain R K 1998 Regulation of transport pathways in tumor vessels: role of tumor type and microenvironment *Proc. Natl Acad. Sci. USA* **95** 4607–12

[41] Jain R K and Stylianopoulos T 2010 Delivering nanomedicine to solid tumors *Nat. Rev. Clin. Oncol.* **7** 653–64

[42] Champion J A, Walker A and Mitragotri S 2008 Role of particle size in phagocytosis of polymeric microspheres *Pharm. Res.* **25** 1815–21

[43] Stewart M P, Lorenz A, Dahlman J and Sahay G 2016 Challenges in carrier-mediated intracellular delivery: moving beyond endosomal barriers *Wiley Interdiscip. Rev. Nanomed. Nanobiotechnol.* **8** 465–78

[44] Albertini J J *et al* 1996 Lymphatic mapping and sentinel node biopsy in the patient with breast cancer *J. Am. Med. Assoc.* **276** 1818–22

[45] Stanton A W, Mellor R H, Cook G J, Svensson W E, Peters A M, Levick J R and Mortimer P S 2003 Impairment of lymph drainage in subfascial compartment of forearm in breast cancer-related lymphedema *Lymphat. Res. Biol.* **1** 121–32

[46] Maeda H, Wu J, Sawa T, Matsumura Y and Hori K 2000 Tumor vascular permeability and the EPR effect in macromolecular therapeutics: a review *J. Control. Release* **65** 271–84

[47] Gabizon A, Shmeeda H and Barenholz Y 2003 Pharmacokinetics of pegylated liposomal Doxorubicin: review of animal and human studies *Clin. Pharmacokinet.* **42** 419–36

[48] Harrington K J, Mohammadtaghi S, Uster P S, Glass D, Peters A M, Vile R G and Stewart J S 2001 Effective targeting of solid tumors in patients with locally advanced cancers by radiolabeled pegylated liposomes *Clin. Cancer Res.* **7** 243–54

[49] Harisinghani M G, Saksena M, Ross R W, Tabatabaei S, Dahl D, McDougal S and Weissleder R 2005 A pilot study of lymphotrophic nanoparticle-enhanced magnetic resonance imaging technique in early stage testicular cancer: a new method for noninvasive lymph node evaluation *Urology* **66** 1066–71

[50] Gabizon A, Isacson R, Rosengarten O, Tzemach D, Shmeeda H and Sapir R 2008 An open-label study to evaluate dose and cycle dependence of the pharmacokinetics of pegylated liposomal doxorubicin *Cancer Chemother. Pharmacol.* **61** 695–702

[51] Tanaka T, Decuzzi P, Cristofanilli M, Sakamoto J H, Tasciotti E, Robertson F M and Ferrari M 2009 Nanotechnology for breast cancer therapy *Biomed. Microdevices* **11** 49–63

[52] Prabhakar U, Maeda H, Jain R K, Sevick-Muraca E M, Zamboni W, Farokhzad O C, Barry S T, Gabizon A, Grodzinski P and Blakey D C 2013 Challenges and key considerations of the enhanced permeability and retention effect for nanomedicine drug delivery in oncology *Cancer Res.* **73** 2412–7

[53] Etheridge M L, Campbell S A, Erdman A G, Haynes C L, Wolf S M and McCullough J 2013 The big picture on nanomedicine: the state of investigational and approved nanomedicine products *Nanomedicine* **9** 1–14

[54] Hafner A, Lovric J, Lakos G P and Pepic I 2014 Nanotherapeutics in the EU: an overview on current state and future directions *Int. J. Nanomed.* **9** 1005–23

[55] Weissig V and Guzman-Villanueva D 2015 Nanopharmaceuticals: II. Products in the pipeline *Int. J. Nanomed.* **10** 1245–57

[56] Weissig V, Pettinger T K and Murdock N 2014 Nanopharmaceuticals: I. Products on the market *Int. J. Nanomed.* **9** 4357–73

[57] Noorlander C W, Kooi M W, Oomen A G, Park M V, Vandebriel R J and Geertsma R E 2015 Horizon scan of nanomedicinal products *Nanomedicine* **10** 1599–608

[58] Evers P 2015 Nanotechnology in Medical Applications: The Global Market, Healthcare Market Research Reports (BCC Research) www.bccresearch.com/market-research/healthcare/nanotechnology-medical-applications-market-hlc069c.html

[59] Duncan R and Gaspar R 2011 Nanomedicine(s) under the microscope *Mol. Pharm.* **8** 2101–41

[60] Barenholz Y 2012 Doxil(R)—the first FDA-approved nano-drug: lessons learned *J. Control. Release* **160** 117–34

[61] O'Shaughnessy J A 2003 Pegylated liposomal doxorubicin in the treatment of breast cancer *Clin. Breast Cancer* **4** 318–28

[62] Singal P K and Iliskovic N 1998 Doxorubicin-induced cardiomyopathy *New Engl. J. Med.* **339** 900–5

[63] Miele E, Spinelli G P, Miele E, Tomao F and Tomao S 2009 Albumin-bound formulation of paclitaxel (Abraxane ABI-007) in the treatment of breast cancer *Int. J. Nanomed.* **4** 99–105

[64] Schroeder A, Avnir Y, Weisman S, Najajreh Y, Gabizon A, Talmon Y, Kost J and Barenholz Y 2007 Controlling liposomal drug release with low frequency ultrasound: mechanism and feasibility *Langmuir* **23** 4019–25

[65] Mazza M, Lozano N, Vieira D B, Buggio M, Kielty C and Kostarelos K 2017 Liposome-indocyanine green nanoprobes for optical labeling and tracking of human mesenchymal stem cells post-transplantation *in vivo Adv. Healthc. Mater.* **1700374** 1–9

[66] Crayton S H, Elias D R, Al Zaki A, Cheng Z and Tsourkas A 2012 ICP-MS analysis of lanthanide-doped nanoparticles as a non-radiative, multiplex approach to quantify biodistribution and blood clearance *Biomaterials* **33** 1509–19

[67] Bligh E G and Dyer W J 1959 A rapid method of total lipid extraction and purification *Can. J. Biochem. Physiol.* **37** 911–7

[68] Tamer Elbayoumi V T 2015 Lipid-based pharmaceutical nanocarriers for imaging applications *Nanotechnology for Biomedical Imaging and Diagnostics: From Nanoparticle Design to Clinical Applications* ed M Y Berezin (New York: Wiley)

[69] Ferlay J, Héry C, Autier P and Sankaranarayanan R 2010 Global burden of breast cancer *Breast Cancer Epidemiology* ed C Li (New York: Springer) pp 1–19

[70] Hanahan D and Weinberg R A 2011 Hallmarks of cancer: the next generation *Cell* **144** 646–74

[71] 2016 What Are the Key Statistics About Breast Cancer A.C. Society https://cancerstatisticscenter.cancer.org

[72] Porter P 2008 'Westernizing' women's risks? Breast cancer in lower-income countries *New Engl. J. Med.* **358** 213–6

[73] Akarolo-Anthony S N, Ogundiran T O and Adebamowo C A 2010 Emerging breast cancer epidemic: evidence from Africa *Breast Cancer Res.* **12** (Suppl. 4) S8

[74] Bianchini G, Balko J M, Mayer I A, Sanders M E and Gianni L 2016 Triple-negative breast cancer: challenges and opportunities of a heterogenous disease *Nat. Rev. Clin. Oncol.* **13** 674–690

[75] Weinberg R 2007 *Biology of Cancer Garland Science* (New York: Taylor & Francis)

[76] Paget S 1889 The distribution of secondary growths in cancer of the breast *Lancet* **133** 571–3

[77] Scott J G, Fletcher A G, Maini P K, Anderson A R and Gerlee P 2014 A filter-flow perspective of haematogenous metastasis offers a non-genetic paradigm for personalised cancer therapy *Eur. J. Cancer* **50** 3068–75

[78] Francia G, Cruz-Munoz W, Man S, Xu P and Kerbel R S 2011 Mouse models of advanced spontaneous metastasis for experimental therapeutics *Nat. Rev. Cancer* **11** 135–41

[79] Immordino M L, Dosio F and Cattel L 2006 Stealth liposomes: review of the basic science, rationale, and clinical applications, existing and potential *Int. J. Nanomed.* **1** 297–315

[80] Davis M E, Zuckerman J E, Choi C H, Seligson D, Tolcher A, Alabi C A, Yen Y, Heidel J D and Ribas A 2010 Evidence of RNAi in humans from systemically administered siRNA via targeted nanoparticles *Nature* **464** 1067–70

[81] Puvanakrishnan P, Park J, Chatterjee D, Krishnan S and Tunnell J W 2012 *In vivo* tumor targeting of gold nanoparticles: effect of particle type and dosing strategy *Int. J. Nanomed.* **7** 1251–8

[82] Chauhan V P, Stylianopoulos T, Martin J D, Popovic Z, Chen O, Kamoun W S, Bawendi M G, Fukumura D and Jain R K 2012 Normalization of tumour blood vessels improves the delivery of nanomedicines in a size-dependent manner *Nat. Nanotechnol.* **7** 383–8

[83] Maeda H and Matsumura Y 2011 EPR effect based drug design and clinical outlook for enhanced cancer chemotherapy preface *Adv. Drug. Deliv. Rev.* **63** 129–30

[84] Hashizume H, Baluk P, Morikawa S, McLean J W, Thurston G, Roberge S, Jain R K and McDonald D M 2000 Openings between defective endothelial cells explain tumor vessel leakiness *Am. J. Pathol.* **156** 1363–80

[85] Folkman J 2001 Can mosaic tumor vessels facilitate molecular diagnosis of cancer? *Proc. Natl Acad. Sci. USA* **98** 398–400

[86] Torchilin V P and Papisov M I 1994 Why do polyethylene glycol-coated liposomes circulate so long? *J. Liposome Res.* **4** 725–39

[87] Blanco E, Shen H and Ferrari M 2015 Principles of nanoparticle design for overcoming biological barriers to drug delivery *Nat. Biotechnol.* **33** 941–51

[88] Corbo C, Molinaro R, Taraballi F, Toledano Furman N E, Hartman K A, Sherman M B, De Rosa E, Kirui D K, Salvatore F and Tasciotti E 2017 Unveiling the *in vivo* protein corona of circulating leukocyte-like carriers *ACS Nano* **11** 3262–73

[89] Cooke V G *et al* 2012 Pericyte depletion results in hypoxia-associated epithelial-to-mesenchymal transition and metastasis mediated by met signaling pathway *Cancer Cell* **21** 66–81

[90] McCarthy N 2012 Leaky effect *Nat. Rev. Cancer* **12** 157

[91] Gnerlich J, Jeffe D B, Deshpande A D, Beers C, Zander C and Margenthaler J A 2007 Surgical removal of the primary tumor increases overall survival in patients with metastatic breast cancer: analysis of the 1988–2003 SEER data *Ann. Surg. Oncol.* **14** 2187–94

[92] Rashid O M and Takabe K 2014 Does removal of the primary tumor in metastatic breast cancer improve survival? *J. Womens Health (Larchmt)* **23** 184–8

[93] Shien T and Doihara H 2014 Resection of the primary tumor in stage IV breast cancer *World J. Clin. Oncol.* **5** 82–5

[94] Cady B, Nathan N R, Michaelson J S, Golshan M and Smith B L 2008 Matched pair analyses of stage IV breast cancer with or without resection of primary breast site *Ann. Surg. Oncol.* **15** 3384–95

[95] Khan S A, Stewart A K and Morrow M 2002 Does aggressive local therapy improve survival in metastatic breast cancer? *Surgery* **132** 620–6

[96] Fidler I J 2003 The pathogenesis of cancer metastasis: the 'seed and soil' hypothesis revisited *Nat. Rev. Cancer* **3** 453–8

[97] Kim M Y, Oskarsson T, Acharyya S, Nguyen D X, Zhang X H, Norton L and Massague J 2009 Tumor self-seeding by circulating cancer cells *Cell* **139** 1315–26

[98] Nguyen D X, Bos P D and Massague J 2009 Metastasis: from dissemination to organ-specific colonization *Nat. Rev. Cancer* **9** 274–84

[99] Norton L and Massague J 2006 Is cancer a disease of self-seeding? *Nat. Med.* **12** 875–8

[100] Leung C T and Brugge J S 2009 Tumor self-seeding: bidirectional flow of tumor cells *Cell* **139** 1226–8

[101] Folkman J and Hochberg M 1973 Self-regulation of growth in three dimensions *J. Exp. Med.* **138** 745–53

[102] Blezinger P *et al* 1999 Systemic inhibition of tumor growth and tumor metastases by intramuscular administration of the endostatin gene *Nat. Biotechnol.* **17** 343–8

[103] Tavazoie S F, Alarcon C, Oskarsson T, Padua D, Wang Q, Bos P D, Gerald W L and Massague J 2008 Endogenous human microRNAs that suppress breast cancer metastasis *Nature* **451** 147–52

[104] Gumireddy K, Li A, Gimotty P A, Klein-Szanto A J, Showe L C, Katsaros D, Coukos G, Zhang L and Huang Q 2009 KLF17 is a negative regulator of epithelial-mesenchymal transition and metastasis in breast cancer *Nat. Cell Biol.* **11** 1297–304

[105] Klein C A 2009 Parallel progression of primary tumours and metastases *Nat. Rev. Cancer* **9** 302–12

[106] O'Reilly M S, Holmgren L, Shing Y, Chen C, Rosenthal R A, Moses M, Lane W S, Cao Y, Sage E H and Folkman J 1994 Angiostatin: a novel angiogenesis inhibitor that mediates the suppression of metastases by a Lewis lung carcinoma *Cell* **79** 315–28

[107] Peinado H *et al* 2017 Pre-metastatic niches: organ-specific homes for metastases *Nat. Rev. Cancer* **17** 302–17

[108] Wheeler S E, Clark A M, Taylor D P, Young C L, Pillai V C, Stolz D B, Venkataramanan R, Lauffenburger D, Griffith L and Wells A 2014 Spontaneous dormancy of metastatic breast cancer cells in an all human liver microphysiologic system *Br. J. Cancer* **111** 2342–50

[109] Milross C G, Tucker S L, Mason K A, Hunter N R, Peters L J and Milas L 1997 The effect of tumor size on necrosis and polarographically measured pO2 *Acta Oncol.* **36** 183–9

[110] Wachsberger P, Burd R and Dicker A P 2003 Tumor response to ionizing radiation combined with antiangiogenesis or vascular targeting agents: exploring mechanisms of interaction *Clin. Cancer Res.* **9** 1957–71

[111] Bhujwalla Z M, Artemov D, Natarajan K, Ackerstaff E and Solaiyappan M 2001 Vascular differences detected by MRI for metastatic versus nonmetastatic breast and prostate cancer xenografts *Neoplasia* **3** 143–53

[112] Sykes E A, Dai Q, Sarsons C D, Chen J, Rocheleau J V, Hwang D M, Zheng G, Cramb D T, Rinker K D and Chan W C 2016 Tailoring nanoparticle designs to target cancer based on tumor pathophysiology *Proc. Natl Acad. Sci. USA* **113** E1142–51

[113] Fass L 2008 Imaging and cancer: a review *Mol. Oncol.* **2** 115–52

[114] Langer R, Brem H, Falterman K, Klein M and Folkman J 1976 Isolations of a cartilage factor that inhibits tumor neovascularization *Science* **193** 70–2

[115] Psaila B and Lyden D 2009 The metastatic niche: adapting the foreign soil *Nat. Rev. Cancer* **9** 285–93

[116] Chambers A F, Groom A C and MacDonald I C 2002 Dissemination and growth of cancer cells in metastatic sites *Nat. Rev. Cancer* **2** 563–72

[117] Nagrath S *et al* 2007 Isolation of rare circulating tumour cells in cancer patients by microchip technology *Nature* **450** 1235–9

[118] Cristofanilli M *et al* 2004 Circulating tumor cells, disease progression, and survival in metastatic breast cancer *New Engl. J. Med.* **351** 781–91

[119] Weis S, Cui J, Barnes L and Cheresh D 2004 Endothelial barrier disruption by VEGF-mediated Src activity potentiates tumor cell extravasation and metastasis *J. Cell Biol.* **167** 223–9

[120] Huang Y, Song N, Ding Y, Yuan S, Li X, Cai H, Shi H and Luo Y 2009 Pulmonary vascular destabilization in the premetastatic phase facilitates lung metastasis *Cancer Res.* **69** 7529–37

[121] Minn A J *et al* 2007 Lung metastasis genes couple breast tumor size and metastatic spread *Proc. Natl Acad. Sci. USA* **104** 6740–5

[122] Hiratsuka S, Ishibashi S, Tomita T, Watanabe A, Akashi-Takamura S, Murakami M, Kijima H, Miyake K, Aburatani H and Maru Y 2013 Primary tumours modulate innate immune signalling to create pre-metastatic vascular hyperpermeability foci *Nat. Commun.* **4** 1853

[123] Kaplan R N *et al* 2005 VEGFR1-positive haematopoietic bone marrow progenitors initiate the pre-metastatic niche *Nature* **438** 820–7